АСТРОФИЗИКА

ТОМ 68 ФЕВРАЛЬ, 2025 ВЫПУСК 1

DOI: 10.54503/0571-7132-2025.68.1-129

A STUDY ON GEODESICS AND LIFESPAN OF THE RINDLER-MODIFIED SCHWARZSCHILD BLACK HOLE. I. TIME-LIKE GEODESICS

T.HUO, C.LIU

Received 12 November 2024
Accepted 14 February 2025

We study the time-like geodesics in the spacetime of the Rindler-modified Schwarzschild black hole (RMSBH) with a cosmological constant. We find that for massive particles, whether undergoing radial motion or orbital motion, are unable to escape the black hole. Meanwhile, at larger orbital radii, the cosmological constant significantly modifies the proper velocity of particles. Additionally, in the case where $\Lambda = 0$, we have presented a special solution: if the particle is located on a specific circular orbit, its proper velocity will remain unaffected by the Rindler acceleration. Furthermore, we discuss the stability of circular orbits by employing the Lyapunov exponent, and draw the dividing line between stable and unstable circular orbits.

Keywords: *Rindler-modified Schwarzschild black hole: cosmological constant: geodesics: circular orbits*

1. *Introduction*. As one of the greatest achievements of classical physics, the General Theory of Relativity (GR) has been widely tested and proven to be correct since its proposal. Among them, many gravitational effects near black holes, such as gravitational redshift [1], perihelion precession [2], light bending [3], quasi-normal modes [4], and gravitational waves [5] can provide tests for GR. The recent release of the first image of a black hole by the Event Horizon Telescope collaboration to the world has further confirming the existence of the most famous celestial bodies predicted by the theory [6]. As we all know, GR is a theory about the geometry of space-time, which explains gravity as the curvature of space-time. Particles will move along geodesics when they are not subjected to any interactions. One of the best ways to investigate the gravitation of a black hole is by studying the particle's motion around it. In fact, the two earliest and most famous verifications of the relativistic effect are the perihelion precession of Mercury and the deflection of light near the sun. There have been extensive studies on the calculation of geodesics around black holes [7-18]. In addition, to investigate the scalar curvature invariants, time-like geodesics or null geodesics are another important criterion for examining the singularity of spacetime. Recently, there have been several interesting results regarding the completeness of geodesics and

spacetime singularities, which one can refer to [19-21].

In fact, our understanding of gravity on a large scale is still not perfect, which is mainly reflected in the problems of cosmological constant and dark matter [22]. The dark matter puzzle originated from Zwicky's observation of the abnormal velocity distribution in the Coma Cluster, where the galaxies were moving at such high speeds that it was difficult for them to remain bound within the cluster. Zwicky pointed out that this might be due to the existence of some matter that we cannot see [23,24]. Another puzzling gravitational anomaly is the anomalous deceleration of the Pioneer spacecraft. Although this deceleration is very slight, it remains unexplained by our current theories. Another explanation for the above-mentioned problem of gravitational behavior at large scales is to modify the existing theories of gravitation. For example, the Modified Newtonian Dynamics (MOND) [25] and $f(R)$ theory [26,27] can, to a certain extent, explain the dark matter problem. In [22], Grumiller proposed an effective model, or the RMSBH model, to explain the anomalous acceleration of the Pioneer spacecraft. In this model, besides the attraction provided by the central celestial body, there is also an additional Rindler term. If the Rindler term is positive, it would also provide an additional attractive force to nearby celestial bodies. This term is directly proportional to r, and thus its effect on the geodesics of particles becomes evident at large distances. Based on this property of the Rindler term, it can explain the rotation curves of local galaxies, making it a possible candidate theory to solve dark matter problem [28]. Lin et al. [29] showed that the Rindler acceleration parameter a in the RMSBH metric plays the role of dark matter. Authors [30-32] further verify the acceleration parameter by considering the HI Nearby Galaxy Survey, and the resulting Rindler acceleration parameter was approximately $a \approx 3 \cdot 10^{-9}\ \mathrm{cm/s^2}$. Iorio [33] considered the Rindler acceleration as a perturbation and computed the effects on the range ρ and range-rate $\dot{\rho}$ between the two bodies in orbital motion. He derived an upper limit for the additional acceleration a_{Rin} provided by the Rindler term, which for the Earth is $7 \cdot 10^{-16}\ \mathrm{m/s^2}$. Carlone et al. [34] discussed the classical tests of general relativity in the presence of Rindler acceleration. In their study, the perihelion shifts, light bending, and gravitational redshift of the solar system planets were calculated. The tightest constraint on Rindler acceleration they obtained, with no caveats, comes from radar echo delay, with the result $|a| < 3\ \mathrm{nm/s^2}$. One can also refer to [35] for the calculation of light bending in the presence of Rindler acceleration. Halilsay et al. [36] further discussed the impact of Rindler acceleration on the radial and circular motions of test particles, including both massive and massless particles.

However, in the aforementioned studies on geodesics for the RMSBH, the influence of the cosmological constant was not taken into account. In such cases, the RMSBH degenerates into the Grumiller-Mazharimousavi-Halilsoy black hole

(GMHBH) [37]. The effect of the cosmological constant on geodesics has been extensively reported, for example, Mohammadi et al. [38] studied the null geodesic of Schwarzschild black hole in anti-de Sitter spacetime with Gaussian matter distribution, Hegde et al. [39] investigated the null Geodesics of four-dimensional Gauss-Bonnet AdS black hole, geodesic motions in AdS Soliton background space-time can be found in [40]. Additionally, black hole thermodynamics, considering the cosmological constant as pressure and introducing extended phase space has significantly expanded the field. Here, we will not delve into the details. For research on black hole thermodynamics in extended phase space, one can refer to [41-50].

The organization of this paper is as follows. In Sections 2 and 3, we will briefly introduce the geometric structure of the RMSBH spacetime and the basic concepts of geodesics, respectively. In Section 4, we will study the geodesics of radial motion of particles in the RMSBH spacetime. Sections 5 and 6 will focus on the geodesics of massive particles in circular orbits. Finally, we summarize and discuss the results and present future prospects. In our study, we consider a positive Rindler acceleration ($a>0$) and a negative cosmological constant ($\Lambda<0$).

2. *Space time structure*. In this section, we will briefly study the space-time structure of a RMSBH. To construct the effective model for gravity of a central object at large scales, Grumiller [22] considered the following four-dimensional spherically symmetric line element

$$ds^2 = g_{\alpha\beta}\left(x^i\right)dx^\alpha dx^\beta + \Phi^2\left(x^i\right)\left(d\theta^2 + \sin^2\theta\, d\varphi^2\right), \tag{1}$$

where the 2-dimensional metric $g_{\alpha\beta}\left(x^i\right)$ and the surface radius $\Phi\left(x^i\right)$ depend only on the coordinates $x^i = \{t, r\}$. To obtain specific solutions for the metric, it is necessary to further describe the dynamics of the field $g_{\alpha\beta}$ and Φ. This is possible in two dimensions, as both the metric g and the scalar field Φ are essentially two-dimensional objects. The process of "spherical reduction" [51] simplifies the 4-dimensional Einstein-Hilbert action to a specific 2-dimensional dilaton gravity model [52]. Grumiller constructed the most general 2-dimensional theory with the field content g and Φ compatible with the following assumptions [22]. First of all, he required the theory to be power-counting renormalizable, assuming that non-renormalizable terms are suppressed. This leads uniquely to the action [53,54]

$$S = -\frac{1}{\kappa^2}\int d^2x\sqrt{-g}\left[f(\Phi)R + 2(\partial\Phi)^2 - 2V(\Phi)\right]. \tag{2}$$

Here, $g = \det\left(g_{\alpha\beta}\right)$ and R is the Ricci scalar. The gravitational coupling constant κ does not play a role in the discussion. Further, Grumiller et al. assumed that the functions f and V are analytic with respect to Φ when Φ is large, as in

spherically eliminated GR [52]. The analysis of the motion equations indicates that, in order to replicate the Newtonian potential -M/r, the coupling function f multiplied by the Ricci scalar R must be specified as $f=\Phi^2$. If considering $f=c\Phi^2$, then the potential energy would transform into $-M/r^{1/c}$, and the experimental constraint on c is $|c-1|<10^{-10}$ [55]. Grumiller [22] conservatively assumed that $f=\Phi^2$ remains unrenormalized in the infrared region, which is highly consistent with experimental data. Next, in fourdimensional terms, Grumiller [22] considered a large surface area surrounding a central object. After spherical reduction, the limit of a large surface area leads to the limit of a large Dilaton field Φ. The potential V is assumed to behave as follows

$$V=\widetilde{\Lambda}\Phi^2+\widetilde{a}\,\Phi+\widetilde{b}+O(1/\Phi). \tag{3}$$

At large Φ, the dominant term of the potential V is quadratic. If higher-order terms of Φ were present, the resulting metric would exhibit curvature singularities at large Φ. By rescaling Φ and κ simultaneously, the subleading coefficients in the asymptotic potential (3) are fixed. Without loss of generality, Grumiller chose $\widetilde{b}=b=2$. By eliminating all asymptotic subleading terms and selecting an appropriate normalization for the coupling constant $\kappa=1$, the action (2) simplifies to [22]

$$S=-\int d^2x\sqrt{-g}\left[\Phi^2 R+2(\partial\Phi)^2-6\Lambda\Phi^2+8a\Phi+2\right], \tag{4}$$

where a and Λ represent the Rindler acceleration and the cosmological constant, respectively. By varying the action (4) and solving the Einstein field equations, one can obtain a spherically symmetric line element as [22,37]

$$ds^2=-f(r)dt^2+f(r)^{-1}dr^2+r^2\left(d\theta^2+\sin^2\theta\,d\varphi^2\right), \tag{5}$$

with

$$f(r)=1-\frac{2M}{r}-\Lambda r^2+2ar. \tag{6}$$

Here, M represents the mass of the black hole and a is the parameter for Rindler acceleration with the range $a<3$ nm/s^2. Λ represents the cosmological constant. It is clear that the black hole solution mentioned above is an extended version of the Schwarzschild-de Sitter solution, or an extension of the Schwarzschild Anti-de Sitter black hole. To examine the singularity of spacetime at the origin of the coordinates, we will proceed to calculate the Kretschmann scalar, which is given by

$$K(r)=R_{\sigma\tau\alpha\beta}R^{\sigma\tau\alpha\beta}=\frac{48M^2}{r^6}+\frac{32a^2}{r^2}-\frac{48a\Lambda}{r}+24\Lambda^2. \tag{7}$$

At the origin, we have $\lim_{r\to 0}K(r)=\infty$, thus, there exists a singularity at the origin. Additionally, the Kretschmann scalar of RMSBH is larger than that of SBH with the same mass. The horizon of the black hole is given by setting $f(r_h)=0$, where

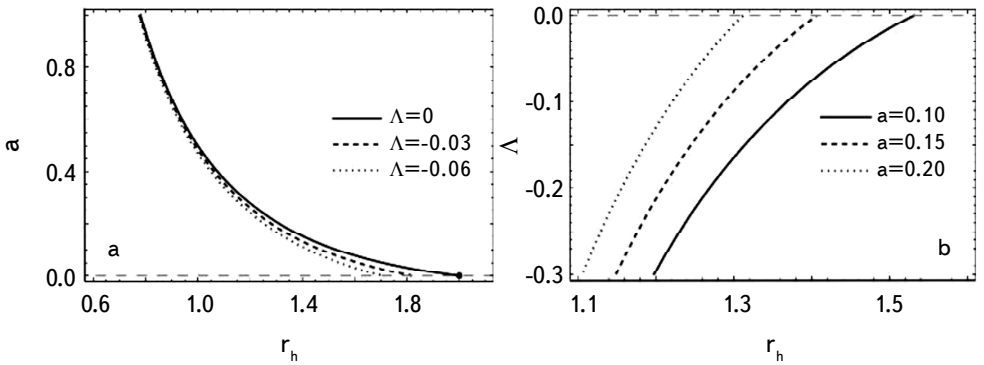

Fig.1. (a) r_h as a function of a for different values of Λ with $M=1$. Black dot denotes the event horizon for the SBH. (b) r_h as a function of Λ for different values of a with $M=1$.

r_h represents the radius of the horizon. As a result, we can obtain the relationship between M and r_h as

$$M=\frac{1}{2}r_h\left(1+2ar_h-\Lambda r_h^2\right). \tag{8}$$

From Eq. (8), we can observe that when $r_h>0$, $r_h\left(1+2ar_h-\Lambda r_h^2\right)/2$ is an increasing function of r_h. Therefore, Eq. (8) will only yield one solution, indicating that the RMSBH has only one horizon. Since the expression of the horizon radius r_h is too complicated, we will not present it here. In Fig.1, we show the trend of r_h changing with a and Λ. It can be observed that as the influence of the acceleration parameter a and the cosmological constant Λ increases, the horizon radius r_h gradually decreases.

3. *Introduction to geodesics.* In order to study the geodesic structure of the spacetime described by (5) and (6), we introduce the following Lagrangian

$$\mathcal{L}=-\frac{1}{2}g_{\mu\nu}\dot{x}^{\mu}\dot{x}^{\nu}, \tag{9}$$

where a dot indicates the derivative with respect to the affine parameter ξ. Combining Eq. (6), we can specifically write the Lagrangian of the RMSBH as

$$\mathcal{L}=\frac{1}{2}\left[f(r)\left(\frac{dt}{d\xi}\right)^2-\frac{1}{f(r)}\left(\frac{dr}{d\xi}\right)^2-r^2\left(\frac{d\theta}{d\xi}\right)^2-r^2\sin^2\theta\left(\frac{d\varphi}{d\xi}\right)^2\right]. \tag{10}$$

Substitute the Lagrangian into the Euler-Lagrange equation

$$\frac{d}{d\tau}\left(\frac{\partial\mathcal{L}}{\partial\dot{x}^{\alpha}}\right)-\frac{\partial\mathcal{L}}{\partial x^{\beta}}=0, \tag{11}$$

we can obtain the equations of motion. Since the RMSBH metric is spherically symmetric, the metric is not a function of the coordinate time t and the rotation

angle φ, so two conserved quantities can be derived from the Lagrangian, namely

$$E = f(r)\left(\frac{dt}{d\xi}\right), \tag{12}$$

$$L = r^2 \sin^2\theta\left(\frac{d\varphi}{d\xi}\right). \tag{13}$$

Here, E and L are two conserved quantities, representing energy and angular momentum, respectively. Generally speaking, E and L are not the quantities measured by static observers in curved spacetime, but rather they are the quantities measured by static observers only at infinity. In addition, we can also obtain an equation for θ through Eq. (10) and Eq. (11)

$$r^2\left(\frac{d^2\theta}{d\xi^2}\right) = r^2\left(\frac{d\varphi}{d\xi}\right)^2 \sin\theta\cos\theta - 2r\left(\frac{dr}{d\xi}\right)\left(\frac{d\theta}{d\xi}\right). \tag{14}$$

Without loss of generality, we adopt the following initial conditions

$$\theta_0 = \frac{\pi}{2}, \quad \frac{d\theta_0}{d\xi} = 0. \tag{15}$$

Hence the angular momentum can be simplified as

$$L = r^2\left(\frac{d\varphi}{d\xi}\right). \tag{16}$$

By choosing the Lagrangian $\mathcal{L} = \eta/2$ and combining with Eq. (10), we can obtain

$$f(r)\left(\frac{dt}{d\xi}\right)^2 - \frac{1}{f(r)}\left(\frac{dr}{d\xi}\right)^2 - r^2\left(\frac{d\theta}{d\xi}\right)^2 - r^2\sin^2\theta\left(\frac{d\varphi}{d\xi}\right)^2 = \eta. \tag{17}$$

Substituting Eq. (12) and Eq. (16) into Eq (17), we can obtain

$$\left(\frac{dr}{d\xi}\right)^2 = E^2 - V_{eff}, \tag{18}$$

where the effective potential is defined as

$$V_{eff} = f(r)\left(\eta + \frac{L^2}{r^2}\right). \tag{19}$$

Eq. (12), Eq. (16), Eq. (18) and Eq. (19) are the basis for studying geodesics.

4. *Radical geodesics*. For time-like geodesics, which represent the motion of massive particles ($\eta = 1$), the effective potential is

$$V_{eff} = 1 - \frac{2M}{r} - \Lambda r^2 + 2ar. \tag{20}$$

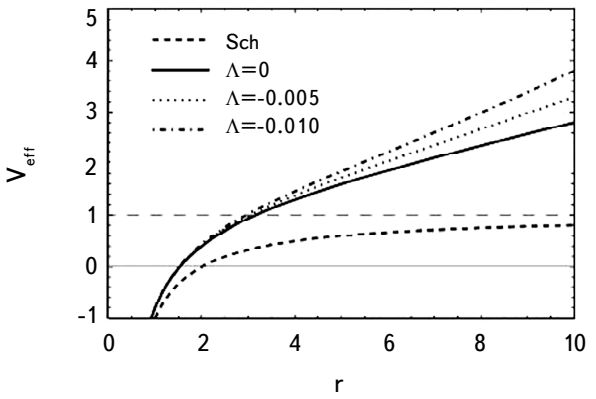

Fig.2. V_{eff} vs r for some Λ with $M=1$, $a=0.1$.

It should be noted that at infinity, the effective potential becomes infinitely large. Therefore, for a massive particle undergoing radial motion, it is impossible for it to escape to infinity. This is a notable difference between RMSBH and SBH, as shown in Fig.2. Additionally, compared to the influence of the Rendler acceleration a on the effective potential energy, the cosmological constant term is proportional to the square of the radius. Therefore, at large distances, the cosmological constant plays a dominant role in governing the motion of particles.

Now, we introduce a test particle to observe its radial motion in the RMSBH spacetime. Our test particle is initially located at $r=r_i$ and is released from rest, thus we have

$$E^2 = V_{eff}(r_i) = 1 - \frac{2M}{r_i} + 2ar_i - \Lambda r_i^2 . \tag{21}$$

By substituting E^2 into Eq. (18), we can obtain the equation of motion for the test particle as

$$\left(\frac{dr}{d\tau}\right)^2 = 2M\left(\frac{1}{r}-\frac{1}{r_i}\right) + 2a(r_i - r) + \Lambda\left(r^2 - r_i^2\right). \tag{22}$$

Therefore, the proper time for the particle to travel from r_i to r is

$$\tau(r) = \int_{r_i}^{r}\left[2M\left(\frac{1}{r}-\frac{1}{r_i}\right) + 2a(r_i - r) + \Lambda\left(r^2 - r_i^2\right)\right]^{-1/2} dr . \tag{23}$$

Furthermore, combining Eq. (12) and Eq. (22), the differential relationship between r and the coordinate time t can be written as

$$\frac{dr}{dt} = \frac{d\tau}{dt}\frac{dr}{d\tau} = \frac{f(r)}{E}\frac{dr}{d\tau} = \frac{f(r)}{E}\sqrt{E^2 - V_{eff}(r)} . \tag{24}$$

Integrating the above equation and combining the initial conditions of the test

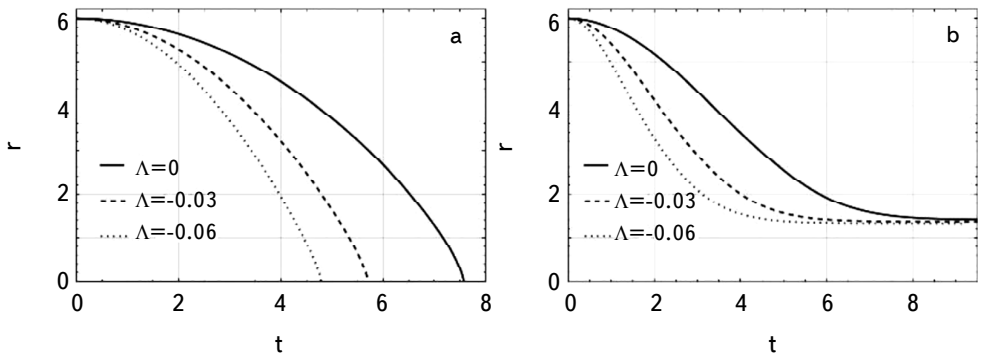

Fig.3. (a) τ vs r for some with Λ with $M=1$, $a=0.15$. (b) The $t(r)$ curve corresponding to (a).

particle, we obtain the coordinate time for the test particle as

$$t(r)=\int_{r_i}^{r}\frac{1}{f(r)}\sqrt{\frac{V_{eff}(r_i)}{V_{eff}(r_i)-V_{eff}(r)}}\,dr\,. \tag{25}$$

As shown in Fig.3a, a test particle is initially stationary at $r_i=6$, after being released, will reach the singularity in a finite proper time. Meanwhile, an increase in the absolute value of cosmological constant will cause the particle to experience less proper time before hitting the singularity, where the geodesic will also terminate. In Fig.3b, it can be observed that as the influence of the cosmological constant increases, an observer at infinity will see the particle approaching the black hole's event horizon in less time, but the particle will never be able to cross the event horizon and enter the black hole.

5. *Orbital geodesics.*

5.1. *The behavior of effective potential for massive particles.* In this section, we will study geodesic motion with $L\neq 0$. Thus, the effective potential is

$$V_{eff}=\left(1-\frac{2M}{r}-\Lambda r^2+2ar\right)\left(1+\frac{L^2}{r^2}\right). \tag{26}$$

For convenience, in this section, we will set $M=1$. Also, we won't provide too many calculations in this section, most of the calculations actually come from the next section. The purpose of this section is to provide a qualitative analysis of the orbital geodesics of massive particles around a RMSBH from the perspective of effective potential. Based on the angular momentum of test particles, the orbital motion can be classified into the following three scenarios:

(1) When $L<4.34$, test particles will eventually fall into the black hole, this this is because $\lim_{r\to\infty}V_{eff}=\infty$, therefore, in this case, there is no escape orbit for

the particle, as shown in Fig.4a;

(2) When $L=4.34$, the innermost stable circular orbit (ISCO) will appear at $r=r_A$, as shown in Fig.4b. Given that the ISCO is an unstable circular orbit, particles on it will eventually fall into the black hole due to even slight perturbations. If the particle is not on the ISCO, it will also eventually fall into the black hole;

(3) When $L>4.34$, if the particle's energy satisfies $E^2=E_1^2$, the particle may be located at $r=r_A$ or may be in a stable circular orbit at $r=r_B$, as shown in Fig.4c. Particles located at $r=r_A$ will inevitably fall into the black hole. Meanwhile, particles on the stable circular orbit, upon experiencing a certain perturbation causing its energy to increase from E_1 to E_2, will move in a bound orbit between perihelion C and aphelion D. If the particle's energy satisfies $E^2=E_3^2$, it may be in an unstable circular orbit at $r=r_E$, and after experiencing a slight perturbation, the particle may either fall into the black hole or move in a bound orbit between r_E and r_F.

Through the above discussion, it can be observed that a notable difference from the SBH spacetime is that particles moving on orbital orbits in the RMSBH spacetime do not possess escape orbits. This is due to the significant changes in the effective potential brought about by the acceleration parameter a and the

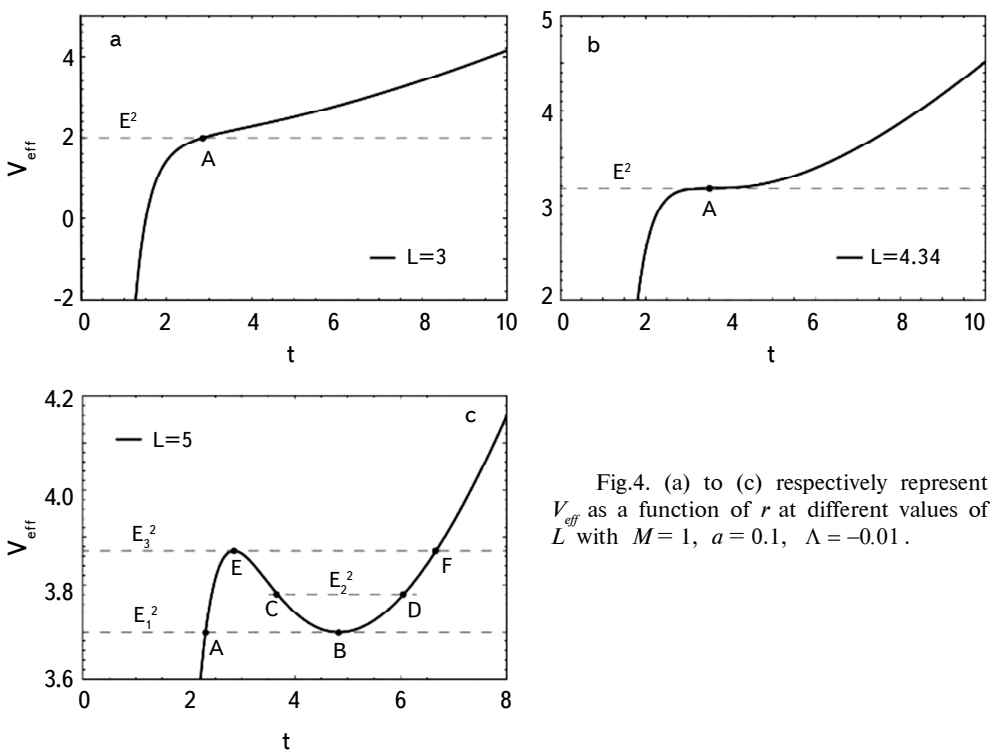

Fig.4. (a) to (c) respectively represent V_{eff} as a function of r at different values of L with $M=1$, $a=0.1$, $\Lambda=-0.01$.

cosmological constant Λ. Meanwhile, compared to the GMHBH, the cosmological constant term in the RMSBH significantly increases the effective potential at large distances. Consequently, the energy required for particles to perform circular motion at these large distances will also increase.

5.2. *Circular orbits*. In this section, we mainly focus on circular time-like orbits. From Eq. (18), we can see that for a particle to maintain a circular orbit, it requires

$$\frac{dr}{d\tau}=0 \quad \text{or} \quad E^2=V_{eff}\,. \tag{27}$$

We notice that under such conditions, the radial proper velocity is

$$v_{pr}=\frac{dl_r}{d\tau}=\left(1-\frac{2M}{r}-\Lambda r^2+2ar\right)^{-1/2}\frac{dr}{d\tau}=0\,, \tag{28}$$

therefore, when a particle moves in a circular orbit, its coordinate distance from the central celestial body remains constant, and so does its proper distance, both of which remain unchanged over time. In the calculation of the aforementioned proper velocity, Eq. (A6) in Appendix A is utilized. Since circular orbits occur at the extrema of the effective potential, we can determine the conditions for a particle to be on a circular orbit by

$$\frac{dV_{eff}}{dr}=\frac{-2L^2\left(-3M+r+ar^2\right)+2r^2\left[M+r^2\left(a-\Lambda r\right)\right]}{r^4}=0\,. \tag{29}$$

Eq. (29) can give the angular momentum that particles on circular orbits need to satisfy

$$L^2=\frac{Mr^2+ar^4-\Lambda r^5}{-3M+r+ar^2}\,. \tag{30}$$

To ensure that $L^2>0$, the radius of the circular orbit must satisfy

$$-3M+r+ar^2>0\,. \tag{31}$$

Thus, we have

$$r>r_b=\frac{6M}{\sqrt{1+12aM}+1}\,, \tag{32}$$

where r_b represents the boundary of the circular orbit radius. Obviously, r_b is a decreasing function of a and is not affected by the cosmological constant. When $a\to 0$, $r_b\to 3M$, corresponding to the case of the SBH. Substituting L^2 into the effective potential (26), we can obtain the effective potential as

$$V_{eff}=\frac{\left[2M+r\left(-1-2ar+\Lambda r^2\right)\right]^2}{r\left(-3M+r+ar^2\right)}\,. \tag{33}$$

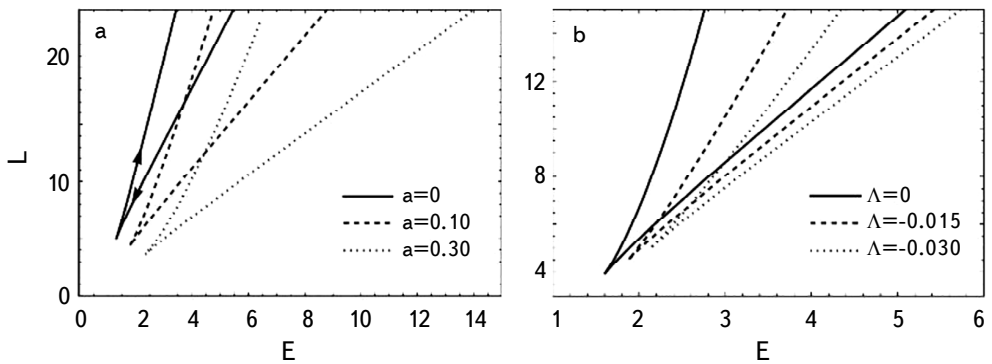

Fig.5. (a) The relationship between the angular momentum and energy of particles located on circular orbits for different values of a with $\Lambda = -0.01$. The arrow direction indicates the increasing direction of r. (b) The relationship between L and E for different values of Λ with $a = 0.1$.

Considering the conditions for circular orbits, we can further derive

$$E^2 = V_{eff} = \frac{\left[2M + r\left(-1 - 2ar + \Lambda r^2\right)\right]^2}{r\left(-3M + r + ar^2\right)}. \tag{34}$$

Using Eq. (30) and Eq. (34), we plotted the relationship between L and E with r as the parameter, as shown in Fig.5. It can be observed that for particles on unstable circular orbits, as the radius r increases, both their energy and angular momentum decrease. The minimum values of energy and angular momentum correspond to the ISCO. After that, as the radius of the circular orbit increases, both the energy and angular momentum of particles on stable circular orbits begin to increase. At the same time, it can be noticed that as the value of a increases, the curve shifts downwards and to the right, while with the increase in the absolute value of Λ, the curve shifts upwards and to the right.

The ISCO refers to the circular orbit with the smallest radius among all stable circular orbits. In addition to satisfying the conditions of Eq. (29), the radius of ISCO r_{ISCO} also needs to meet $d^2V_{eff}/dr_{ISCO}^2 = 0$, namely,

$$6M^2 - Mr_{ISCO} + 12aMr_{ISCO}^2 + \left(-3a - 15\Lambda M\right)r_{ISCO}^3 + \left(-2a^2 + 4\Lambda\right)r_{ISCO}^4 + 3a\Lambda r_{ISCO}^5 = 0, \tag{35}$$

the solution is

$$\Lambda = \frac{-6M^2 + ar_{ISCO}^3\left(3 + 2ar_{ISCO}\right) + M\left(r_{ISCO} - 12ar_{ISCO}^2\right)}{r_{ISCO}^3\left(-15M + 4r_{ISCO} + 3ar_{ISCO}^2\right)}. \tag{36}$$

This is the condition that the r_{ISCO} of a RMSBH satisfies. Setting $\Lambda = 0$, we can derive the r_{ISCO} of a GMHBH satisfies

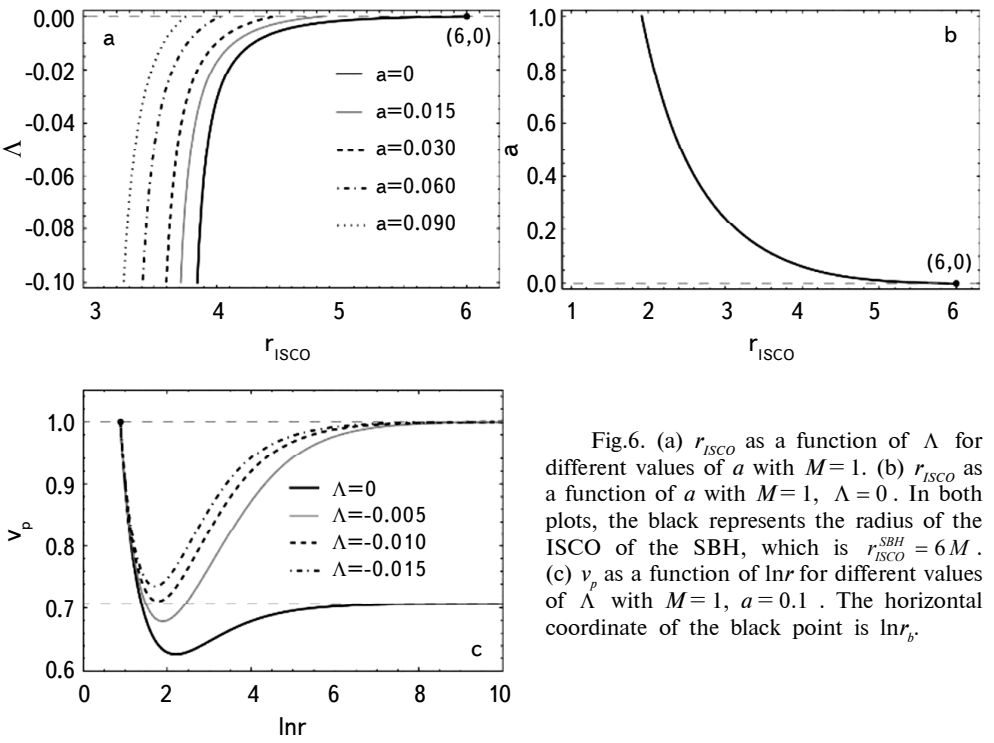

Fig.6. (a) r_{ISCO} as a function of Λ for different values of a with $M=1$. (b) r_{ISCO} as a function of a with $M=1$, $\Lambda=0$. In both plots, the black represents the radius of the ISCO of the SBH, which is $r_{ISCO}^{SBH}=6M$. (c) v_p as a function of ln$r$ for different values of Λ with $M=1$, $a=0.1$. The horizontal coordinate of the black point is lnr_b.

$$a=\frac{12M-3r_{ISCO}+\sqrt{192M^2-80Mr_{ISCO}+9r_{ISCO}^2}}{4r_{ISCO}^2}. \tag{37}$$

Further setting $a=0$ in Eq. (37), we can get the radius of the ISCO of a SBH, which is $r_{ISCO}^{SBH}=6M$ [56]. As can be seen from Fig.6a, the radius of the ISCO decreases with the increase of the absolute value of the cosmological constant, so compared with the GMHBH of the same mass, the RMSBH has a smaller radius of the ISCO. Similarly, as shown in Fig.6b, the radius of the ISCO of the RMSBH decreases with the increase of a. Therefore, we have the following relationship: $r_{ISCO}^{RMSBH}<r_{ISCO}^{GMHBH}<r_{ISCO}^{SBH}$.

Next, we will continue to find out the angular velocity Ω of the particles moving in circular orbits. Substituting Eq. (34) into Eq. (12), we can obtain

$$\frac{dt}{d\tau}=\frac{E}{f(r)}=\sqrt{\frac{r}{-3M+r+ar^2}}. \tag{38}$$

On the other hand, combining Eq. (30) and Eq. (16), we can obtain

$$\frac{d\varphi}{d\tau}=\frac{L}{r^2}=\frac{1}{r}\sqrt{\frac{M+r^2(a-\Lambda r)}{-3M+r+ar^2}}. \tag{39}$$

Thus, the angular velocity is

$$\Omega^{RMSBH}=\frac{d\varphi}{dt}=\frac{d\varphi}{d\tau}\frac{d\tau}{dt}=\sqrt{\frac{M+ar^2}{r^3}-\Lambda}\,. \tag{40}$$

By setting $\Lambda=0$, Ω degrades to the GMHBH scenario. Further setting $a=0$, we can get the radius of the angular velocity of the SBH: $\Omega^{SBH}=\sqrt{M/r^3}$. Obviously, in Eq. (40), Ω^{RMSBH} is an increasing function of a and Λ, therefore we have: $\Omega^{RMSBH}>\Omega^{GMHBH}>\Omega^{SBH}$.

With the angular velocity at hand, we can derive the proper velocity of a particle moving on a circular orbit, which can be expressed as

$$v_p^{RMSBH}=\frac{1}{\sqrt{f(r)}}\left(r\frac{d\varphi}{dt}\right)=\frac{r\Omega^{RMSBH}}{\sqrt{f(r)}}=\sqrt{\frac{M+r^2(a-\Lambda r)}{-2M+r+2ar^2-\Lambda r^3}}\,. \tag{41}$$

In the process of calculating (41), we used Eq. (A7) in Appendix A. Regarding proper velocity, as shown in Fig.6c, the relationship is as follows: $v_p^{RMSBH}>v_p^{GMHBH}$. When r approaches r_b, both the proper velocities of RMSBH and GMHBH tend to unity, which is the speed of light, indicating that their circular orbit radii must be larger than r_b. The difference lies in the fact that, due to the influence of the cosmological constant, v_p^{RMSBH} tends to the speed of light at infinity. In contrast, v_p^{GMHBH} tends to $\sqrt{2}/2$.

For a GMHBH, Eq. (41) can be rewritten in the following form

$$\left[2\left(v_p^{GMHBH}\right)^2-1\right]ar^2+\left(v_p^{GMHBH}\right)^2r-\left[2\left(v_p^{GMHBH}\right)^2+1\right]M=0 \tag{42}$$

If $v_p^{GMHBH}=1/\sqrt{2}$, then the coefficient of a in the above equation will vanish, and we have $r=4M$. This interesting solution indicates that regardless of the value of a, the proper velocity v_p^{RMSBH} at $r=4M$ is always $1/\sqrt{2}$. From Fig.7a, we can observe that as r increases, v_p^{RMSBH} first decreases and then increases, approaching

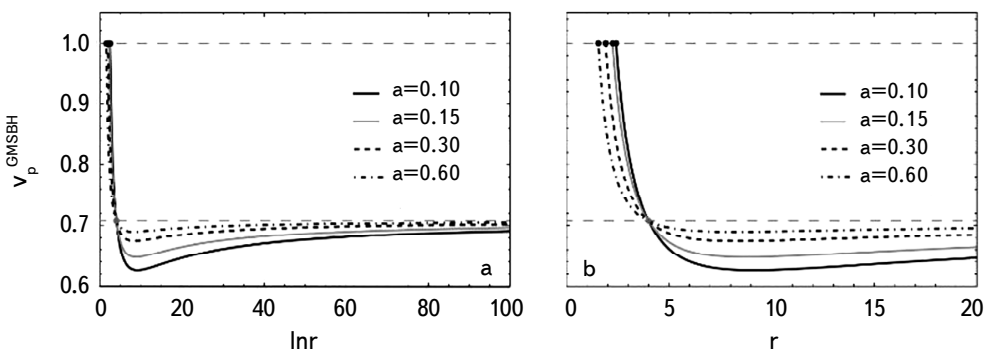

Fig.7. (a) v_p as a function of r for some different values of a, with $M=1$. (b) The local enlargement of (a), with the grey point having coordinates $(4, 1/\sqrt{2})$.

$1/\sqrt{2}$ at infinity. Fig.7b allows us to observe the special solution mentioned above. The proper velocity curve in the SBH scenario also passes through this point.

5.3. *Lyapunov exponent for circular time-like orbits*. In this section, we use Lyapunov exponent as a measure of the stability of circular orbit. The Lyapunov exponent can measure the average convergence rate or divergence rate of nearby orbits in phase space [57]. In general, a real Lyapunov exponent indicates that nearby orbits are divergent, while an imaginary Lyapunov exponent indicates that nearby orbits are convergent. When the Lyapunov exponent vanishes, it indicates that the orbit is critically stable. The Lyapunov exponent in coordinate time is given by [58]

$$\lambda = \sqrt{-\frac{V''_{eff}(r)}{2[\dot{t}(r)]^2}}, \tag{43}$$

where r is the radius of the circular orbits. With this definition, we can derive the Lyapunov exponent for circular orbits around a RMSBH as

$$\lambda^{RMSBH} = \frac{1}{r^2}\sqrt{6M^2 - Mr\left(1 - 12ar + 15\Lambda r^2\right) + r^3\left[-2a^2 r + 4\Lambda r + 3a\left(-1 + \Lambda r^2\right)\right]}\ . \tag{44}$$

Setting $\Lambda = 0$, Eq. (44) degenerates into the Lyapunov exponent for a

$$\lambda^{GMHBH} = \frac{1}{r^2}\sqrt{6M^2 - Mr\left(1 - 12ar\right) + r^3\left(-3a - 2a^2 r\right)}\ . \tag{45}$$

It can be easily verified that by setting $a = 0$ in Eq. (45), we can obtain the Lyapunov exponent for the SBH. The black line in Fig.8a represents $\lambda^{RMSBH} = 0$, with the region to its right (λ^{RMSBH} is a complex number) indicating the area of stable circular orbits, and the region to its left indicating the area of unstable

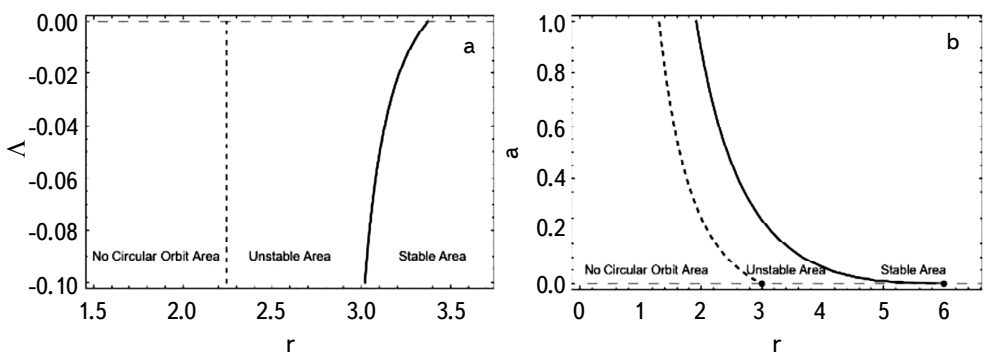

Fig.8. (a) The black line represents $\lambda^{RMSBH} = 0$, which is the dividing line between stable circular orbits and unstable circular orbits. The dashed line represents r_b, which is not a function of Λ, hence it is a straight line. (b) The trend of the stable and unstable circular orbit regions of the GMHBH varying with a is depicted, with horizontal the black dashed line representing the scenario for the SBH. In both figures, we set $M = 1$.

circular orbits. It is important to note that the radius of circular orbits need to satisfy the condition of $r > r_b$. Therefore, unstable circular orbits are located in the region between the black line and the dashed line. It can be observed that as the absolute value of the cosmological constant increases, the region of unstable circular orbits gradually shrinks, and r_{ISCO} shifts towards the left. Fig.8b shows the trend of the Lyapunov exponent of the GMHBH varying with a. Similarly, the region of stable circular orbits expands to the left. However, unlike the previous case, the radius r_b also contracts towards the left as a increases, resulting in an overall leftward contraction of the unstable circular orbit region.

6. *Conclusions*. In this paper, we studied the time-like geodesics of RMSBH. It is found that, due to the introduction of acceleration parameter a and cosmological constant Λ, a massive particle undergoing radial motion cannot escape the black hole and will ultimately fall into it. Similarly, massive particles in circular orbits are also unable to escape the black hole to infinity, which significantly differ from the scenario in a SBH. Furthermore, for particles in circular motion, we derived their effective potential V_{eff}, energy E, angular velocity Ω, proper velocity v_p, and coordinate velocity v_c. Both the acceleration parameter and the cosmological constant are found to increase the coordinate velocity of the particles. Interestingly, for a GMHBH, we uncovered a unique solution: the acceleration parameter a does not affect the proper velocity of particles orbiting on the $r = 4M$ circular orbit.

Additionally, regarding the time-like geodesics, we discussed the stability of circular orbits by employing the Lyapunov exponent, and drew the dividing line between stable and unstable circular orbits.

Acknowledgments. The work was supported by the Natural Science Foundation of Zhejiang Province of China (No.LY14A030001).

Department of Physics, Shaoxing University, Shaoxing 312000,
China, e-mail: czlbj20@163.com

APPENDIX A

The spacetime geometry is of essential to the motion of particles within it. Therefore, we will briefly introduce the spacetime geometry of a RMSBH. In a four-dimensional curved spacetime, the proper spatial distance is defined as

$$dl = \sqrt{\gamma_{ij}\, dx^i dx^j}\ , \quad (i, j = 1, 2, 3) \tag{A1}$$

in which

$$\gamma_{ij} = g_{ij} - \frac{g_{0i}g_{0j}}{g_{00}}. \tag{A2}$$

Here, γ_{ij} is defined as spatial metric. By substituting the line element (3) into the definition, we can find the proper distances along the r, θ, and φ directions in a RMSBH, respectively, as

$$dl_r = \left(1 - \frac{2M}{r} - \Lambda r^2 + 2ar\right)^{-1/2} dr, \quad dl_\theta = r d\theta, \quad dl_\varphi = r\sin\theta d\varphi. \tag{A3}$$

If we set $dr=0$ in the line element (3), we can obtain the line element for surface of constant r as

$$dl_s^2 = r^2\left(d\theta^2 + \sin^2\theta d\varphi^2\right). \tag{A4}$$

It is obvious that (A4) is identical to the line element for a spherical surface in threedimensional flat space. The proper time and coordinate time of a RMSBH have the following relationship

$$d\tau = \sqrt{-g^{00}}\, dt = \left(1 - \frac{2M}{r} - \Lambda r^2 + 2ar\right)^{1/2} dt. \tag{A5}$$

Based on this, the radial proper velocity and tangential proper velocity of a particle are, respectively

$$v_{pr} = \frac{dl_r}{d\tau} = \left(1 - \frac{2M}{r} - \Lambda r^2 + 2ar\right)^{-1} \frac{dr}{dt}, \tag{A6}$$

$$v_{ps} = \frac{dl_s}{d\tau} = \frac{r\sqrt{d\theta^2 + \sin^2\theta d\varphi^2}}{\left(1 - \frac{2M}{r} - \Lambda r^2 + 2ar\right)^{1/2} dt}. \tag{A7}$$

ИССЛЕДОВАНИЕ ГЕОДЕЗИЧЕСКИХ ЛИНИЙ И ВРЕМЕНИ СУЩЕСТВОВАНИЯ МОДИФИЦИРОВАННОЙ РИНДЛЕРОМ ЧЕРНОЙ ДЫРЫ ШВАРЦШИЛЬДА. I. ВРЕМЕНИПОДОБНЫЕ ГЕОДЕЗИЧЕСКИЕ ЛИНИИ

Т.ХО, Ч.ЛЮ

Исследованы времениподобные геодезические линии в пространственно-временной метрике модифицированной Риндлером черной дыры Шварцшильда (RMSBH) с учетом космологической постоянной. Установлено, что массивные частицы, находящиеся в радиальном или орбитальном движении, не могут

покинуть черную дыру. Между тем на больших радиусах орбит космологическая постоянная существенно влияет на собственную скорость частиц. Кроме того, в случае, когда $\Lambda = 0$, представлено особое решение: если частица находится на определенной круговой орбите, ее собственная скорость останется неизменной под воздействием ускорения Риндлера. Также анализирована устойчивость круговых орбит, используя показатель Ляпунова, и определена граница между устойчивыми и неустойчивыми круговыми орбитами.

Ключевые слова: *модифицированная Риндлером черная дыра Шварцшильда: космологическая постоянная: геодезические линии: круговые орбиты*

REFERENCES

1. *D.K.Ross*, Il Nuovo Cimento B, **2**, 55, 1971.
2. *R.Greenberg*, Astron. J., **86**, 912, 1981.
3. *V.A. De Lorenci*, *N.Figueiredo*, *H.H.Fliche et al.*, Astron. Astrophys., **369**, 690, 2001.
4. *V.Cardoso*, *R.Konoplya*, *J.P.S.Lemos*, Phys. Rev. D, **68**, 044024, 2003.
5. *B.P.Abbott*, *R.Abbott*, *T.D.Abbott et al.*, Phys. Rev. Lett., **116**, 061102, 2016.
6. The Event Horizon Telescope Collaboration, APJL, **L1**, 875, 2019.
7. *G.Sanzeni*, J. Math. Phys., **65**, 082503, 2024.
8. *M.Heydari-Fard*, *M.Heydari-Fard*, Int. J. Mod. Phys. D, **31**, 2250066, 2022.
9. *S.Giri*, *H.Nandan*, Gen. Relativ. Gravity, **53**, 76, 2021.
10. *A.Ramos*, *C.Arias*, *R.Ávalos et al.*, Ann. Phys., **431**, 168557, 2021.
11. *J.P.Hu*, *Y.Zhang*, *Li-LiShi et al.*, Gen. Relativ. Gravity, **50**, 89, 2018.
12. *M.A.A.Paula*, *L.C.S.Leite*, *L.C.B.Crispino*, Phys. Rev. D, **102**, 104033, 2020.
13. *T.C.Frost*, *V.Perlick*, Class. Quantum Grav., **38**, 085016, 2021.
14. *A.Das*, *A.Saha*, *S.Gangopadhyay*, Class. Quantum Grav., **38**, 065015, 2021.
15. *L.Herrera*, *A. Di Prisco*, *J.Ospino et al.*, Phys. Rev. D, **101**, 064071, 2020.
16. *R.Carballo-Rubio*, *F. Di Filippo*, *S.Liberati et al.*, Phys. Rev. D, **101**, 084047, 2020.
17. *S.W.Wei*, *Y.X.Liu*, Chinese Phys. C, **44**, 115103, 2020.
18. *M.Momennia*, *S.H.Hendi*, Phys. Rev. D, **99**, 124025, 2019.
19. *T.Zhou*, *L.Modesto*, Phys. Rev. D, **107**, 044016, 2023.
20. *M.E.Rodrigues*, *H.A.Vieira*, Eur. Phys. J. Plus, **138**, 974, 2023.
21. *M.Guerrero*, *G.J.Olmo*, *D.Rubiera-Garcia*, Eur. Phys. J. C, **83**, 785, 2023.
22. *D.Grumiller*, Phys. Rev. Lett. **105** 211303 (2010).
23. *F.Zwicky*, Helvetica Physica Acta, **6**, 110, 1933.
24. *F.Zwicky*, Astrophys. J., **86**, 217, 1937.
25. *M.Milgrom*, Astrophys. J., **270**, 365, 1983.

26. *S.Capozziello*, *V.F.Cardone*, *A.Troisi*, Mon. Not. Roy. Astron. Soc., **375**, 1423, 2007.
27. *T.P.Sotiriou*, *V.Faraoni*, Rev. Mod. Phys., **82**, 451, 2010.
28. *H.N.Lin*, *M.H.Li*, *X.Li et al.*, Mon. Not. Roy. Astron. Soc., **430**, 450, 2013.
29. *S.H.Mazharimousavi*, *M.Halilsoy*, Mod. Phys. Lett. A, **28**, 1350073, 2013.
30. *F.Walter et al.*, Astron. J., **136**, 2563, 2008.
31. *J.Mastache*, *J.L.Cervantes-Cota*, *A. de la Macorra*, Phys. Rev. D, **87**, 063001, 2013.
32. *J.L.Cervantes-Cota*, *J.A.Gomez-Lopez*, Phys. Lett. B, **728**, 537, 2014.
33. *L.Iorio*, JCAP, **05**, 019, 2011.
34. *S.Carloni*, *D.Grumiller*, *F.Preis*, Phys. Rev. D, **83**, 124024, 2011.
35. *J.Sultana*, *D.Kazanas*, Phys. Rev. D, **85**, 081502(R), 2012.
36. *M.Halilsoy*, *O.Gurtug*, *S.H.Mazharimousavi*, Gen. Relativ. Gravity, **45**, 2363, 2013.
37. *S.Mandal*, *S.Das*, *D.J.Gogoi et al.*, Phys. Dark. Universe Phys., **42**, 101349, 2023.
38. *A.Mohammadi*, *N.Doustimotlagh*, *T.Golanbari et al.*, arXiv:2101.08842v3.
39. *K.Hegde*, *A.N.Kumara*, *C.L.Rizwan et al.*, Ann. Phys., **429**, 168461, 2021.
40. *H.Q.Shi*, *D.F.Zeng*, arXiv:1603.08624v1.
41. *D.Kubiznak*, *R.B.Mann*, JHEP, **1207**, 033, 2012.
42. *W.Javed*, *Z.Yousaf*, *Z.Akhtar*, Mod. Phys. Lett. A, **33**, 1850089, 2018.
43. *F.Simovic*, *I.Soranidis*, Phys. Rev. D, **109**, 044029, 2024.
44. *Y.Guo*, *H.Xie*, *Y.G.Miao*, Nucl. Phys. B, **1000**, 116491, 2024.
45. *S.Murk*, *I.Soranidis*, Phys. Rev. D, **108**, 044002, 2023.
46. *D.V.Singh*, *S.Siwach*, Phys. Lett. B, **808**, 135658, 2020.
47. *P.Paul*, *S.Upadhyay*, *D. Veer Singh*, Eur. Phys. J. Plus, **138**, 6, 2023.
48. *S.I.Kruglov*, Grav. Cosmol., **29**, 57, 2023.
49. *M.Chabab*, *H.ElMoumni*, *S.Iraoui et al.*, LHEP, **2**, 02, 2018.
50. *C.Li*, *P.Z.He*, *P.Li et al.*, Gen. Relativ. Gravity, **52**, 50, 2020.
51. *B.K.Berger*, *D.M.Chitre*, *V.E.Moncrief et al.*, Phys. Rev. D, **5**, 2467, 1972.
52. *D.Grumiller*, *W.Kummer*, *D.V.Vassilevich*, Phys. Rep., **369**, 327, 2002.
53. *J.G.Russo*, *A.A.Tseytlin*, Nucl. Phys. B, **382**, 259, 1992.
54. *S.D.Odintsov*, *I.L.Shapiro*, Phys. Lett. B, **263**, 183, 1991.
55. *C.Talmadge*, *J.P.Berthias*, *R.W.Hellings et al.*, Phys. Rev. Lett., **61**, 1159, 1988.
56. *V.Ferrari*, *L.Gualtieri*, *P.Pani*, General relativity and its Applications:Black Holes, Compact Stars and Gravitational Waves, CRC Press, Boca Raton London New York, p.192, 2020.
57. *A.AI-Badawi*, *M.Q.Owaidat*, Gen. Relativ. Gravity, **55**, 131, 2023.
58. *V.Cardoso*, *A.S.Miranda*, *E.Berti et al.*, Phys. Rev. D, **79**, 064016, 2009.